

## Experimental and Theoretical Studies on the Aqueous Solvation and Reactivity of $\text{SmCl}_2$ and Comparison with $\text{SmBr}_2$ and $\text{SmI}_2$

Alejandro Ramírez-Solís,<sup>\*,†,‡,§</sup> Caroline O. Bartulovich,<sup>‡</sup> César Iván León-Pimentel,<sup>§</sup> Humberto Saint-Martin,<sup>§</sup> William R. Anderson, Jr.,<sup>‡</sup> and Robert A. Flowers II<sup>\*,‡,§</sup>

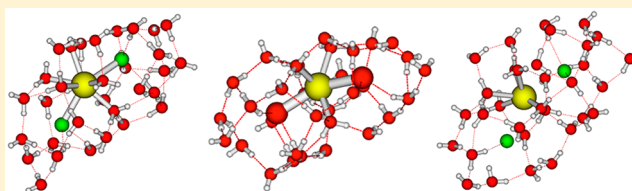
<sup>†</sup>Departamento de Física, Centro de Investigación en Ciencias-IICBA Universidad Autónoma del Estado de Morelos, Cuernavaca, Morelos 62209, Mexico

<sup>‡</sup>Department of Chemistry, Lehigh University, Bethlehem, Pennsylvania 18015, United States

<sup>§</sup>Instituto de Ciencias Físicas, UNAM, Cuernavaca, Morelos 62210, Mexico

### S Supporting Information

**ABSTRACT:** Water addition to Sm(II) has been shown to increase reactivity for both  $\text{SmI}_2$  and  $\text{SmBr}_2$ . Previous work in our groups has demonstrated that this increase in reactivity can be attributed to coordination induced bond weakening enabling substrate reduction through proton-coupled electron transfer. The present work examines the interaction of water with samarium dichloride ( $\text{SmCl}_2$ ) and illustrates the importance of the Sm–X interaction and bond distance upon water addition critical for the reactivity of the reagent system. Born–Oppenheimer molecular dynamics simulations identify substantial variations among the reductants created in solution upon water addition to  $\text{SmI}_2$ ,  $\text{SmBr}_2$ , and  $\text{SmCl}_2$  with the latter showing the least halide dissociation. This results in a lower water coordination number for  $\text{SmCl}_2$ , creating a more powerful reducing system. As previously shown with the other  $\text{SmX}_2$ –water systems, coordination-induced bond-weakening of the O–H bond of water bound to Sm(II) results in significant bond weakening. In the case of  $\text{SmCl}_2$ , the bond weakening is estimated to be in the range of 83 to 88.5 kcal/mol.



Born–Oppenheimer molecular dynamics simulations identify substantial variations among the reductants created in solution upon water addition to  $\text{SmI}_2$ ,  $\text{SmBr}_2$ , and  $\text{SmCl}_2$  with the latter showing the least halide dissociation. This results in a lower water coordination number for  $\text{SmCl}_2$ , creating a more powerful reducing system. As previously shown with the other  $\text{SmX}_2$ –water systems, coordination-induced bond-weakening of the O–H bond of water bound to Sm(II) results in significant bond weakening. In the case of  $\text{SmCl}_2$ , the bond weakening is estimated to be in the range of 83 to 88.5 kcal/mol.

## INTRODUCTION

Samarium diiodide ( $\text{SmI}_2$ ) is an important reductant in the arsenal of synthetic chemists and has been rigorously studied and broadly utilized over the past 4 decades.<sup>1–3</sup> Proton donors, such as water and alcohols, have been shown to have a significant impact on both the selectivity and reactivity of Sm(II)-based reductants.<sup>4,5</sup> Proton donors are one of the most widely used additive classes, with water being shown to have both a significant and unique effect on these reactions.<sup>6,7</sup> When used in conjunction with water,  $\text{SmI}_2$  is capable of reducing a wide range of functionalities as well as initiate a variety of bond-forming reactions and reductive cyclizations.<sup>8–11</sup>

Other Sm(II) reductants, such as samarium dibromide ( $\text{SmBr}_2$ ) and samarium dichloride ( $\text{SmCl}_2$ ), have been less utilized until recently but have found applications in synthesis for reductions, reductive couplings, and reductive cyclizations.<sup>12–14</sup> These reagents can be easily produced through the addition of several equivalents of the lithium or ammonium halide salts but have limited solubility in comparison to  $\text{SmI}_2$ .<sup>15</sup> Recent work in our groups focusing on  $\text{SmBr}_2$  demonstrated that the addition of water leads to significant weakening of the O–H bond of water coordinated to  $\text{SmBr}_2$ , similar to that previously observed for  $\text{SmI}_2$ –water.<sup>7</sup> Unlike with the  $\text{SmI}_2$ –water system, the halide ions do not dissociate from the  $\text{SmBr}_2$ –water system to the same extent creating a unique reductant in solution. This system is less stable than that

formed with  $\text{SmI}_2$ –water and will evolve hydrogen gas if left for substantial periods of time.<sup>7</sup> Given previous work, we sought to understand the interaction of water with  $\text{SmCl}_2$  in comparison to other  $\text{SmX}_2$ –water systems and the impact of O–H bond-weakening on the reactivity of the  $\text{SmCl}_2$ –water complex.

## CHARACTERIZATION OF THE $\text{SmCl}_2$ –WATER SYSTEM

Like  $\text{SmBr}_2$ ,  $\text{SmCl}_2$  can be prepared in multiple ways.<sup>15–17</sup> The most straightforward approach which is utilized in most synthetic studies uses the addition of lithium chloride (LiCl) to an existing solution of  $\text{SmI}_2$ .<sup>15</sup> For our reactions we utilized the ammonium halide salt, tetrabutylammonium chloride (TBACl) as opposed to LiCl for preparation of  $\text{SmCl}_2$  due to its increased solubility. Both of these methods generate  $\text{SmCl}_2$  with identical UV–vis spectra.<sup>18</sup>

Water has been shown to have a high affinity for Sm(II) based on previous studies of  $\text{SmI}_2$  and  $\text{SmBr}_2$ .<sup>7,19,20</sup> In both cases, coordination of water displaces bound solvent even at low concentrations resulting in an observable shift in the UV–vis spectrum.<sup>7,21</sup> A similar shift for  $\text{SmCl}_2$  would be indicative of water coordination to the Sm(II) metal center. To

Received: June 18, 2019

investigate the impact of the addition of water to  $\text{SmCl}_2$ , a series of UV–vis spectra were taken and examined with increasing concentrations of water versus a 2.5 mM solution of  $\text{SmCl}_2$ . This can be seen in Figure 1.

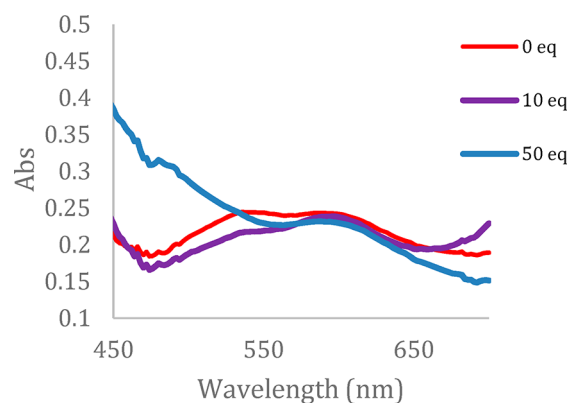


**Figure 1.** UV–vis spectra of 2.5 mM  $\text{SmCl}_2$  in THF containing 0, 10, and 50 equiv of water vs  $[\text{SmCl}_2]$ .

**Computational Studies.** To address the aqueous solvation of  $\text{SmCl}_2$  and gain insight into the speciation of the  $\text{SmCl}_2$ –water complex, Born–Oppenheimer molecular dynamics (BOMD) Density Functional Theory (DFT) simulations were carried out on the  $\text{SmCl}_2$ – $(\text{H}_2\text{O})_{32}$  model system and compared with both the  $\text{SmBr}_2$ – $(\text{H}_2\text{O})_{32}$ <sup>7</sup> and  $\text{SmI}_2$ – $(\text{H}_2\text{O})_{32}$  systems.<sup>22</sup> The BOMD simulations were carried out with Geraldyn-2.1<sup>23</sup> coupled to Gaussian 09.<sup>24</sup> The BOMD simulations were done at 300 K using the same NVT scheme<sup>25,26</sup> as that applied for  $\text{SmBr}_2$ – $(\text{H}_2\text{O})_{32}$ <sup>7</sup> and  $\text{SmI}_2$ – $(\text{H}_2\text{O})_{32}$ .<sup>22</sup> Details on the time step, (O,H) atomic basis sets, the hybrid density functional, and the electronic structure and energy/gradient calculations can be found in refs 7 and 22. The chlorine and samarium atoms were treated with 7 and 10 active valence electrons as described previously.<sup>7,27,28</sup> The optimized  $\text{SmCl}_2$  structure provided the initial Sm–Cl distance ( $R_c(\text{Sm–Cl}) = 2.61$ ) used. Initial velocity vectors were determined by the thermal energy using a Boltzmann distribution at 300 K. The 25 ps (50 000 system configurations) BOMD simulation on the lowest singlet potential surface required 9088 CPU days. A reliable thermalization period of 10 ps was utilized here. Structural, dynamic, and energetic data were extracted from the last 15 ps of the trajectory to perform the statistical analysis. Radial distribution functions (RDFs) for Sm–O and Sm–Cl were obtained, providing the corresponding coordination numbers (CN) as functions of distance to the metal.

The EXAFS spectrum from the molecular dynamics trajectory was obtained using the same procedure<sup>29</sup> as that used for the aqueous solvation of  $\text{SmBr}_2$ ,<sup>7</sup>  $\text{SmI}_2$ ,<sup>22</sup> and  $\text{SmI}_3$ .<sup>30</sup> A total of 500 decorrelated snapshots were used to obtain the theoretical EXAFS spectrum. The same cutoff (5.0 Å) centered around the Sm atom was applied as in our previous studies using the FEFF program<sup>31</sup> (version 9.03) with an amplitude reduction factor  $S_0^2 = 1$ .

**Analysis of the BOMD Simulation.** Figure 2 shows a typical microsolvation pattern for  $\text{SmCl}_2$ . Figure 3 shows the evolution of the total potential energy during the whole simulation. Thermalization was achieved in 20 000 steps because the slope of the linear fit of the water binding energy for the last 15 ps is  $-1.7 \times 10^{-4}$  au/ps.

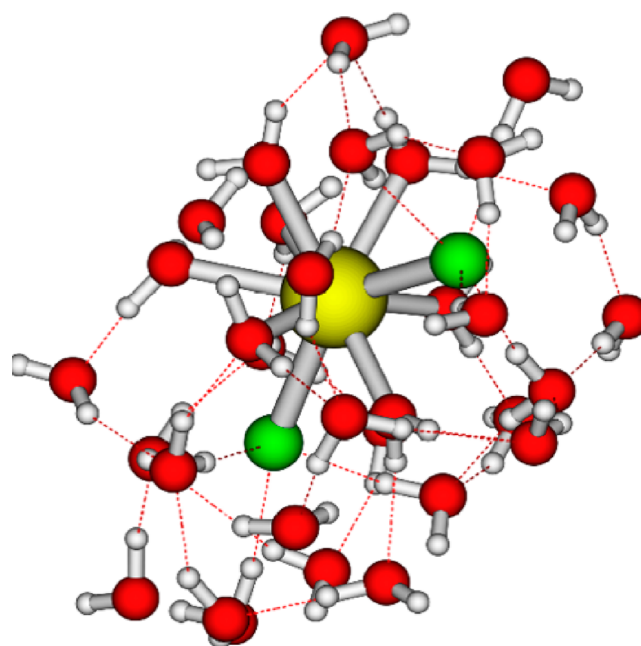


**Figure 2.** Microsolvation pattern for the  $\text{SmCl}_2$ – $(\text{H}_2\text{O})_{32}$  system at 300 K upon thermalization. Sm (yellow), O (red), and Cl atoms (green).

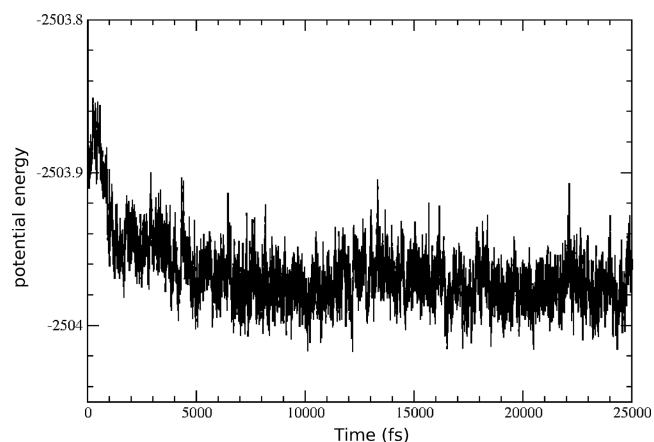


**Figure 3.** Evolution of the total potential energy (au) for the  $\text{SmCl}_2$ – $(\text{H}_2\text{O})_{32}$  system at 300 K.

The  $\text{SmI}_2$ ,  $\text{SmBr}_2$ ,<sup>7</sup> and  $\text{SmCl}_2$  BOMD simulations were carried out using identical microsolvation conditions, and the evolution of the Sm–X distances was compared for the  $\text{SmI}_2$ – $(\text{H}_2\text{O})_{32}$  and  $\text{SmBr}_2$ – $(\text{H}_2\text{O})$  systems described previously.<sup>7,22</sup> This data is contained in Figure 4.

These plots reveal unique differences among the halogens with respect to the Sm(II) metal center under the same simulation conditions. For  $\text{SmI}_2$ , rapid displacement of the iodide occurs with one of the iodide ions remaining between the first and the second water solvation shells (ca. 3.6 Å), while the second is displaced to an average distance of 5.5 Å: the free space left leads to a coordination number of 8.4 for water in the coordination sphere of Sm(II). For  $\text{SmBr}_2$  the bromide anions do not fully dissociate from Sm(II), and both are contained within the first and the second solvation shells of Sm(II) at an average distance (3.3 Å). In this case, the lower degree of bromide dissociation leads to a smaller water coordination number CN = 7.5. In the  $\text{SmCl}_2$  system, both

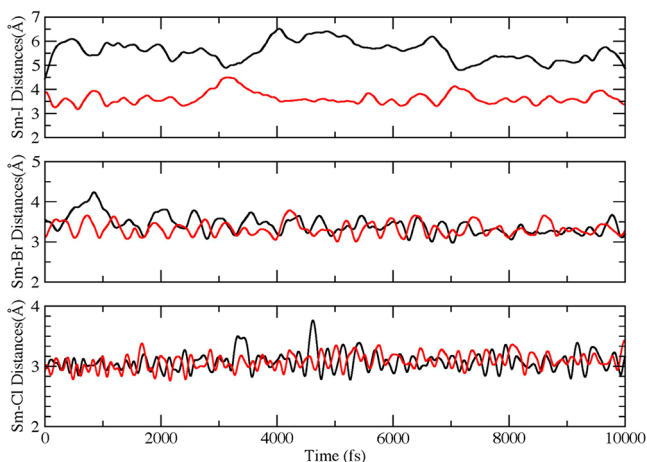


**Figure 4.** Comparison of the evolution of the Sm–I<sup>22</sup> (top), Sm–Br<sup>7</sup> (middle), and Sm–Cl (bottom) distances for the SmX<sub>2</sub>–(H<sub>2</sub>O)<sub>32</sub> systems at 300 K. For each system the two Sm–X distances are shown (red and black). Note the different scales and the increasing frequency of oscillation in the sequence SmX<sub>2</sub> (X = I, Br, Cl).

chloride anions remain tightly bound to Sm(II) at a substantially shorter average distance (3.1 Å) lying within the first solvation shell. This allows only five water molecules to come close to the Sm(II), resulting in a smaller coordination number CN = 6.8. Table 1 summarizes these comparisons among the three systems.

**Table 1.** Average Sm–X Distances and Water Coordination Numbers for the SmX<sub>2</sub>–(H<sub>2</sub>O)<sub>32</sub> Systems at 300 K

SmX <sub>2</sub> system	average Sm–X (Å)	CN
SmI <sub>2</sub>	4.67	8.5
SmBr <sub>2</sub>	3.31	7.5
SmCl <sub>2</sub>	3.11	6.8

In order to quantitatively compare the solvation environments around the SmCl<sub>2</sub>, SmBr<sub>2</sub>, and SmI<sub>2</sub> reagents, the Sm–O and Sm–X (X = Cl, Br, I) RDFs acquired from the last 10 ps of each BOMD trajectory are contained in Figure 5. The first solvation shell extends from 2.7 to 3.4 Å, and integration leads to a coordination number CN = 6.8 water molecules around the Sm(II) cation, approximately two fewer than found for the SmI<sub>2</sub>–water system. The second solvation sphere extends from 3.3 to approximately 5 Å. The feature at 5.2 Å is likely a consequence of the superposition of the second and third solvation shells.

The average Sm–Cl distances (3.1 Å) in the water microsolvated system are slightly longer than the Sm–Cl equilibrium distance of the non-solvated molecule (2.6 Å). In addition, the angle of the Cl–Sm–Cl remains relatively close to that of the isolated molecule ca. 140° (see Figure 6). These data are consistent with a much stronger metal–halide interaction in this case.

A full geometry optimization of the SmCl<sub>2</sub>–(H<sub>2</sub>O)<sub>32</sub> system was carried out from the lowest energy structure of the BOMD simulation, to understand the lower activity of SmCl<sub>2</sub> as performed in previous studies of the SmI<sub>2</sub>–(H<sub>2</sub>O)<sub>32</sub> and SmBr<sub>2</sub>–(H<sub>2</sub>O)<sub>32</sub> systems.<sup>7</sup> Figure 7 contains the optimized microsolvated systems (at 0 K) at the same level of theory. When examining the SmX<sub>2</sub>–(H<sub>2</sub>O)<sub>32</sub> systems, there are several quantities of interest that are useful to compare: (1) the Sm–X

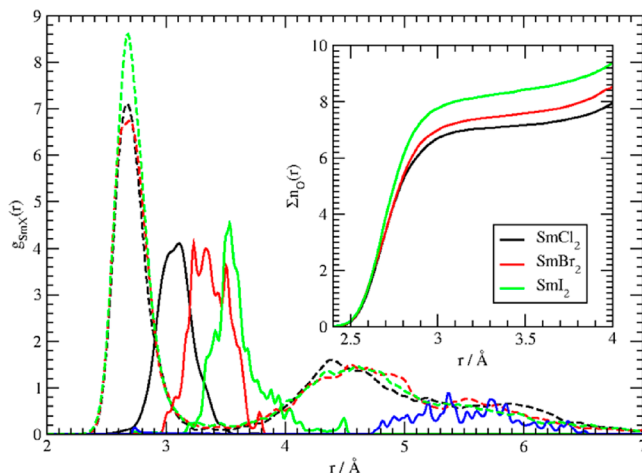


**Figure 5.** Radial distribution functions  $g_{\text{SmX}}(r)$ . Solid lines are used for the halides Cl (black), Br (red), and I (green), with peaks successively displaced to the right. Note that one of the I atoms completely detached from Sm(II) (blue line). Dashed lines are used for  $g_{\text{SmO}}(r)$  in each case. The number of coordinated oxygens (inset) increases as the distance from the halide to Sm becomes longer; note the clear hierarchy with increasing atomic number of the halogen.

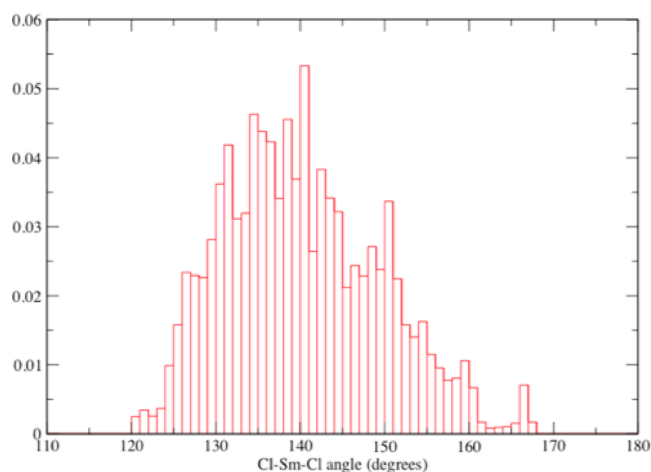


**Figure 6.** Distribution of the Cl–Sm–Cl angle for microsolvated SmCl<sub>2</sub> at 300 K. The average angle is nearly identical to that of the isolated SmCl<sub>2</sub> molecule showing the much stronger Sm(II)–Cl<sup>−</sup> ionic interaction in this case.

optimized distances, (2) the associated CN number of Sm-bonded water molecules, (3) the total water binding energies, and (4) the natural charges of the Sm and halogen ions. Since the evolution of metal–ligand charge transfer (MLCT)<sup>32</sup> is a function of the halogen, we determined the natural charges of the Sm and of the halogen ions through Natural Population Analyses (NPA) as shown in Table 2.

Although the optimal SmI<sub>2</sub>–(H<sub>2</sub>O)<sub>32</sub> structure contains six water molecules coordinated to Sm(II), for the SmBr<sub>2</sub> only five water molecules interact with Sm(II). However, the optimal SmCl<sub>2</sub>–(H<sub>2</sub>O)<sub>32</sub> cluster contains six water molecules around the Sm(II). Though this might seem contradictory to the trend found for I and Br, it is due to the fact that SmCl<sub>2</sub> allows one more water molecule than SmBr<sub>2</sub> at 0 K because the ionic radius of the chloride is significantly smaller than that of the bromide, thus creating a larger solid angle around Sm(II) where water oxygens can bind to the metal. This fact is clearly

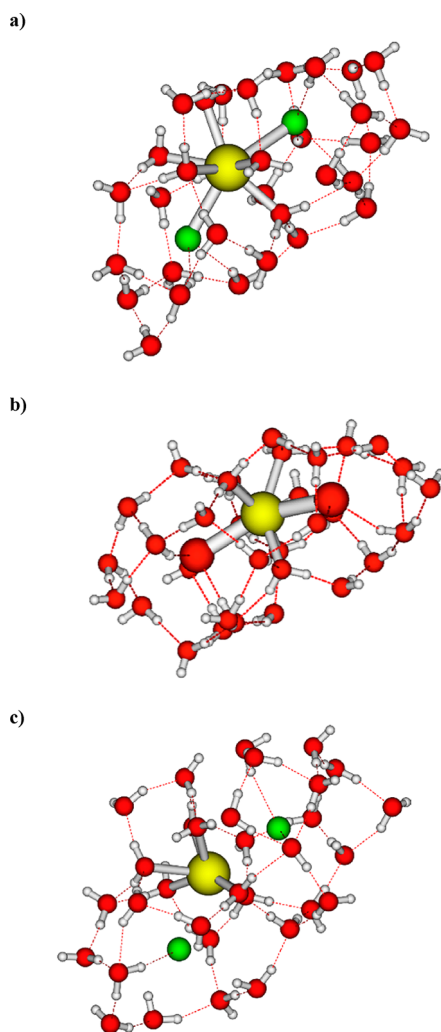


**Figure 7.** Optimized geometries for the microsolvated (a)  $\text{SmCl}_2-(\text{H}_2\text{O})_{32}$ , (b)  $\text{SmBr}_2-(\text{H}_2\text{O})_{32}$ ,<sup>7</sup> (middle), and (c)  $\text{SmI}_2-(\text{H}_2\text{O})_{32}$  systems.<sup>22</sup>

**Table 2. Summary of Significant Quantities Determined for the Optimized  $\text{SmX}_2-(\text{H}_2\text{O})_{32}$  Systems: Optimized Sm–X Distances (Å), Water Binding Energies (kcal/mol), Water Coordination Number (CN), and Natural Population Charges on Sm and X**

parameter	$\text{SmCl}_2-(\text{H}_2\text{O})_{32}$	$\text{SmBr}_2-(\text{H}_2\text{O})_{32}$	$\text{SmI}_2-(\text{H}_2\text{O})_{32}$
Sm–X distances	2.91, 3.01	3.04, 3.16	3.32, 3.38
CN	6	5	6
binding energy	–19.03	–18.42	–17.74
NPA charge Sm	0.750	0.859	0.744
NPA charge X1	–0.703	–0.697	–0.628
NPA charge X2	–0.694	–0.673	–0.607

linked to the larger NPA charge on Sm(II) for the  $\text{SmBr}_2-(\text{H}_2\text{O})_{32}$  optimized cluster as compared to the  $\text{SmCl}_2$  and  $\text{SmI}_2$  cases. Also noteworthy is the decreasing natural charge on the halide ions in the sequence chlorides (ca. 0.70 e), bromides (ca. 0.68e), and iodides (ca. 0.62e), in agreement with the previous results. It is interesting to note that the NPA revealed a slight positive charge (+0.03e to +0.05e) on all the Sm-coordinated water molecules in the microsolvated environment; a table in the Supporting Information shows the natural charges on the six coordinated water molecules.

The calculated EXAFS spectrum is shown in Figure S9 in the Supporting Information. To the best of our knowledge to date, no experimental EXAFS data have been reported for  $\text{SmCl}_2$  in water. As a consequence, comparisons can be made only qualitatively with our theoretical prediction with that obtained for  $\text{SmI}_2$  and with the experimental EXAFS spectrum reported for Sm(III).

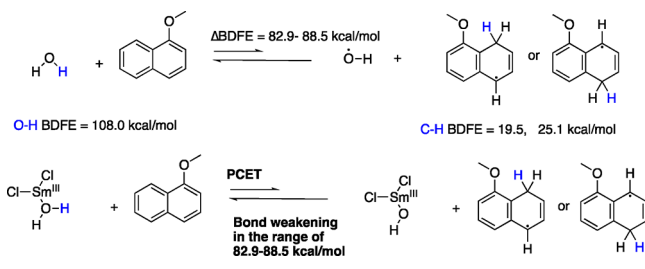
The data from BOMD simulations at 300 K demonstrate important differences between  $\text{SmI}_2$ –water and  $\text{SmCl}_2$ –water. These differences are a consequence of a number of factors including the different local dynamic hydration patterns for  $\text{SmCl}_2$  and  $\text{SmI}_2$ , the larger charge of Cl vs I in the lowest energy optimized  $\text{SmX}_2-(\text{H}_2\text{O})_{32}$  complexes, and the larger total binding energy of chloride for Sm(II) that inhibits dissociation in the microsolvation environment.

With the knowledge gleaned from these computational studies, we sought to explore the limit of reduction that could be achieved with  $\text{SmCl}_2$ –water through the reduction of a series of arenes that are significantly more difficult to reduce. It was found that reduction of 1-methoxynaphthalene was achieved (see SI). However, arenes more difficult to reduce with more negative reduction potentials, such as biphenyl, were unable to be reduced.

Although strong coordination of water to  $\text{SmCl}_2$  results in an increase in reactivity, it also leads to a decrease in the stability of the system due to the competing formation of  $\text{H}_2$ . As a consequence, kinetic studies were not feasible even though the reagent system can be used synthetically if performed appropriately. As an example in  $\text{SmCl}_2$ –water system reactions, 2 equiv of water based on  $[\text{Sm}(\text{II})]$  are used whereas in the  $\text{SmBr}_2$ –water system reactions over 30 equiv of water are employed. This change in reaction design diminishes the competing formation of  $\text{H}_2$  and optimizes product yield.

The instability of the  $\text{SmCl}_2-\text{H}_2\text{O}$  complex is a result of the O–H bond weakening of water that results from coordination to the strong reductant. The extent of O–H bond weakening of water when coordinated to  $\text{SmCl}_2$  was estimated through the reduction of a series of arenes that were increasingly more difficult to reduce. We found that phenanthrene was reduced in an 80% yield and that 1-methoxynaphthalene was the limit with reduction of 5–10%. Density functional theory (DFT) calculations, as described in previous publications, were used to determine BDFEs of the intermediate radicals that would be formed via a hydrogen atom transfer (HAT) to 1-methoxynaphthalene.<sup>33,34</sup> The minimum degree of bond weakening for this radical intermediate to be formed can be determined by subtracting the O–H BDFE from the C–H BDFE of the arene radical formed upon HAT to 1-methoxynaphthalene. Therefore, in this case, the bond weakening of the O–H bond of water when bound to  $\text{SmCl}_2$  can be estimated to be 83–88.5 kcal/mol. Using this logic, this provides a BDFE for water bound to  $\text{SmCl}_2$  of approximately 19.5–25.1 kcal/mol (Scheme 1).<sup>6</sup> This concept of bond-weakening of various ligands when bound to low-valent metals is one that is well-established for other reductants.<sup>35–40</sup> Previous work has shown that, for both  $\text{SmI}_2$  and  $\text{SmBr}_2$ , the coordination of water results in a substantial bond weakening of 73 and 83 kcal/mol, respectively.<sup>9,7</sup> The present results demonstrate a more substantial bond weakening for the  $\text{SmCl}_2-\text{H}_2\text{O}$  complex. This estimate of the degree of bond weakening shows that the combination of  $\text{SmCl}_2$  and water provides a powerful reagent

**Scheme 1. Approximation of the Minimum Degree of O–H Bond Weakening upon Coordination of Water to SmCl<sub>2</sub> in THF**



that is able to facilitate the formation of extremely weak C–H bonds upon formal HAT to substrates.

## CONCLUSIONS

The data obtained in these studies demonstrates that the addition of water to SmCl<sub>2</sub> results in the formation of an extremely powerful reductant. Furthermore, the identity of the halide ligand on Sm(II) has a significant effect on the coordination of water and the reactivity of the resulting reducing complex. In the case of SmCl<sub>2</sub>, it was found that both chloride ions remain very tightly bonded to the metal, more so than with SmBr<sub>2</sub>, to Sm(II) with none of them leaving the first solvation sphere. Similar to SmBr<sub>2</sub>, upon increasing amounts of water, chloride ions are not liberated to the same degree that occurs with SmI<sub>2</sub>. The trend in reactivity between the SmX<sub>2</sub>–H<sub>2</sub>O systems corresponds well to the water coordination sphere in each case. The water coordination sphere is strongly dependent on the attractive ionic Sm–X interaction, which changes significantly depending on the halide used. The stronger the interaction between the halide and the Sm(II) metal center, the stronger the halides are held allowing less water molecules to coordinate, thereby reducing the effective coordination number. Having the halides remain bound with the coordinated water produces a more powerful reducing system. The coordination of water to SmCl<sub>2</sub> leads to substantial O–H bond-weakening in the range of 83–88.5 kcal/mol. This bond weakening leads to substrate reduction through a proton-coupled electron transfer mechanism. Overall, the importance of proton donor coordination and Sm(II)–halide ionic interaction illustrates that this method can be used to form extremely weak C–H bonds, as shown in Scheme 1, that can be used to facilitate endergonic reactions thought to be well outside of the range of Sm(II)-based reductants. We are currently examining the impact of coordination of other O–H and N–H proton donors to Sm(II), and the results from these studies will be presented in due course.

## ASSOCIATED CONTENT

### Supporting Information

The Supporting Information is available free of charge on the ACS Publications website at DOI: 10.1021/acs.inorgchem.9b01818.

General experimental methods; spectroscopic, rate, and computational data (PDF)

## AUTHOR INFORMATION

### Corresponding Authors

\*E-mail: alex@uaem.mx.

\*E-mail: rof2@lehigh.edu.

### ORCID

Alejandro Ramírez-Solís: 0000-0002-8428-5714

Humberto Saint-Martin: 0000-0003-4159-6165

Robert A. Flowers, II: 0000-0003-2295-1336

### Notes

The authors declare no competing financial interest.

## ACKNOWLEDGMENTS

R.A.F. is grateful to the National Science Foundation (CHE1565741) for support of this work. A.R.-S. acknowledges support from CONACYT Basic Science project number 253679. H.S.-M. acknowledges financial support from DGAPA-UNAM grant no. IN110419.

## REFERENCES

- Molander, G. A.; Harris, C. R. Sequencing Reactions with Samarium (II) Iodide. *Chem. Rev.* **1996**, *96*, 307–338.
- Edmonds, D. J.; Johnston, D.; Procter, D. J. Samarium(II)-Iodide-Mediated Cyclizations in Natural Product Synthesis. *Chem. Rev.* **2004**, *104*, 3371–3403.
- Szostak, M.; Fazakerley, N. J.; Parmar, D.; Procter, D. J. Cross-Coupling Reactions Using Samarium(II) Iodide. *Chem. Rev.* **2014**, *114*, 5959–6039.
- Chciuk, T. V.; Anderson, W. R.; Flowers, R. A., II High-Affinity Proton Donors Promote Proton-Coupled Electron Transfer by Samarium Diodide. *Angew. Chem., Int. Ed.* **2016**, *55*, 6033–6036.
- Amiel-Levy, M.; Hoz, S. Guidelines for the Use of Proton Donors in SmI<sub>2</sub> Reactions: Reduction of  $\alpha$ -Cyanostilbene. *J. Am. Chem. Soc.* **2009**, *131*, 8280–8284.
- Chciuk, T. V.; Flowers, R. A., II Proton-Coupled Electron Transfer in the Reduction of Arenes by SmI<sub>2</sub> – Water Complexes. *J. Am. Chem. Soc.* **2015**, *137*, 11526–11531.
- Ramírez-Solís, A.; Bartulovich, C. O.; Chciuk, T. V.; Hernández-Cobos, J.; Saint-Martin, H.; Maron, L.; Anderson, W. R.; Li, A. M.; Flowers, R. A., II Experimental and Theoretical Studies on the Implications of Halide-Dependent Aqueous Solvation of Sm(II). *J. Am. Chem. Soc.* **2018**, *140*, 16731–16739.
- Szostak, M.; Spain, M.; Procter, D. J. Ketyl-Type Radicals from Cyclic and Acyclic Esters Are Stabilized by SmI<sub>2</sub>(H<sub>2</sub>O)<sub>n</sub>: The Role of SmI<sub>2</sub>(H<sub>2</sub>O)<sub>n</sub> in Post-Electron Transfer Steps. *J. Am. Chem. Soc.* **2014**, *136*, 8459–8466.
- Chciuk, T. V.; Anderson, W. R.; Flowers, R. A., II Reversibility of Ketone Reduction by SmI<sub>2</sub> – Water and Formation of Organosamarium Intermediates. *Organometallics* **2017**, *36*, 4579–4583.
- Szostak, M.; Spain, M.; Parmar, D.; Procter, D. J. Selective Reductive Transformations Using Samarium Diodide-Water. *Commun.* **2012**, *48*, 330–346.
- Just-Baringo, X.; Procter, D. J. Sm(II)-mediated electron transfer to carboxylic acid derivatives: Development of complexity-generating cascades. *Acc. Chem. Res.* **2015**, *48*, 1263–1275.
- Huang, H. M.; Procter, D. J. Dearomatizing Radical Cyclizations and Cyclization Cascades Triggered by Electron-Transfer Reduction of Amide-Type Carbonyls. *J. Am. Chem. Soc.* **2017**, *139*, 1661–1667.
- Lebrun, A.; Namy, J. L.; Kagan, H. B. Samarium Dibromide an Efficient Reagent for the Pinacol Coupling Reactions. *Tetrahedron Lett.* **1993**, *34*, 2311–2314.
- Szostak, M.; Spain, M.; Procter, D. J. Determination of the Effective Redox Potentials of SmI<sub>2</sub>, SmBr<sub>2</sub>, SmCl<sub>2</sub>, and Their Complexes with Water by Reduction of Aromatic Hydrocarbons. Reduction of Anthracene and Stilbene by Samarium(II) Iodide-Water Complex. *J. Org. Chem.* **2014**, *79*, 2522–2537.
- Fuchs, J. R.; Mitchell, M. L.; Shabangi, M.; Flowers, R. A. The Effect of Lithium Bromide and Lithium Chloride on the Reactivity of SmI<sub>2</sub> in THF. *Tetrahedron Lett.* **1997**, *38*, 8157–8158.

- (16) Héllion, F.; Lannou, M. I.; Namy, J. L. A New Preparation of Samarium Dibromide and Its Use in Stoichiometric and Catalytic Pinacol Coupling Reactions. *Tetrahedron Lett.* **2003**, *44*, 5507–5510.
- (17) Dahlén, A.; Hilmersson, G. Microwave-Assisted Generation of Lanthanide(II) Halides in THF and Simple Quantitative Determination. *Eur. J. Inorg. Chem.* **2004**, *2004* (15), 3020–3024.
- (18) Miller, R. S.; Sealy, J. M.; Shabangi, M.; Kuhlman, M. L.; Fuchs, J. R.; Flowers, R. A., II Reactions of SmI<sub>2</sub> with Alkyl Halides and Ketones: Inner-Sphere vs Outer-Sphere Electron Transfer in Reactions of Sm(II) Reductants. *J. Am. Chem. Soc.* **2000**, *122*, 7718–7722.
- (19) Prasad, E.; Flowers, R. A., II Mechanistic Impact of Water Addition to SmI<sub>2</sub>: Consequences in the Ground and Transition State. *J. Am. Chem. Soc.* **2005**, *127*, 18093–18099.
- (20) Chopade, P. R.; Prasad, E.; Flowers, R. A., II The Role of Proton Donors in SmI<sub>2</sub>-Mediated Ketone Reduction: New Mechanistic Insights. *J. Am. Chem. Soc.* **2004**, *126*, 44–45.
- (21) Sadasivam, D. V.; Teprovich, J. A.; Procter, D. J.; Flowers, R. A., II Dynamic Ligand Exchange in Reactions of Samarium Diiodide. *Org. Lett.* **2010**, *12*, 4140–4143.
- (22) Ramírez-Solís, A.; Amaro-Estrada, J. I.; Hernández-Cobos, J.; Maron, L. Aqueous Solvation of SmI<sub>2</sub>: A Born-Oppenheimer Molecular Dynamics Density Functional Theory Cluster Approach. *J. Phys. Chem. A* **2017**, *121*, 2293–2297.
- (23) Raynaud, C.; Maron, L.; Daudey, J. P.; Jolibois, F. Reconsidering Car-Parrinello Molecular Dynamics Using Direct Propagation of Molecular Orbitals Developed upon Gaussian Type Atomic Orbitals. *Phys. Chem. Chem. Phys.* **2004**, *6*, 4226–4232.
- (24) Frisch, M. J.; Trucks, G. W.; Schlegel, H. B.; Scuseria, G. E.; Robb, M. A.; Cheeseman, J. R.; Scalmani, G.; Barone, V.; Mennucci, B.; Petersson, G. A.; Nakatsuji, H.; Caricato, M.; Li, X.; Hratchian, H. P.; Izmaylov, A. F.; Bloino, J.; Zheng, G.; Sonnenberg, J. L.; Hada, M.; Ehara, M.; Toyota, K.; Fukuda, R.; Hasegawa, J.; Ishida, M.; Nakajima, T.; Honda, Y.; Kitao, O.; Nakai, H.; Vreven, T.; Montgomery, J. A., Jr.; Peralta, J. E.; Ogliaro, F.; Bearpark, M.; Heyd, J. J.; Brothers, E.; Kudin, K. N.; Staroverov, V. N.; Kobayashi, R.; Normand, J.; Raghavachari, K.; Rendell, A.; Burant, J. C.; Iyengar, S. S.; Tomasi, J.; Cossi, M.; Rega, N.; Millam, J. M.; Klene, M.; Knox, J. E.; Cross, J. B.; Bakken, V.; Adamo, C.; Jaramillo, J.; Gomperts, R.; Stratmann, R. E.; Yazyev, O.; Austin, A. J.; Cammi, R.; Pomelli, C.; Ochterski, J. W.; Martin, R. L.; Morokuma, K.; Zakrzewski, V. G.; Voth, G. A.; Salvador, P.; Dannenberg, J. J.; Dapprich, S.; Daniels, A. D.; Farkas, O.; Foresman, J. B.; Ortiz, J. V.; Cioslowski, J.; Fox, D. J. *Gaussian 09*; Gaussian, Inc.: Wallingford, CT, 2009.
- (25) Nosé, S. A Unified Formulation of the Constant Temperature Molecular Dynamics Methods. *J. Chem. Phys.* **1984**, *81*, 511–519.
- (26) Hoover, W. G. Canonical Dynamics: Equilibrium Phase-Space Distributions. *Phys. Rev. A: At., Mol., Opt. Phys.* **1985**, *31*, 1695–1697.
- (27) Bergner, A.; Dolg, M.; Küchle, W.; Stoll, H.; Preuß, H. Ab Initio Energy-Adjusted Pseudopotentials for Elements of Groups 13–17. *Mol. Phys.* **1993**, *80*, 1431–1441.
- (28) Dolg, M.; Stoll, H.; Preuß, H.; Pitzer, R. M. Relativistic and Correlation Effects for Element 105 (hahnium, Ha): A Comparative Study of M and MO (M= Nb, Ta, Ha) Using Energy-Adjusted Ab Initio Pseudopotentials. *J. Phys. Chem.* **1993**, *97*, 5852.
- (29) Merkling, P. J.; Muñoz-Páez, A.; Martínez, J. M.; Pappalardo, R. R.; Sánchez Marcos, E. Molecular-Dynamics-Based Investigation of Scattering Path Contributions to the EXAFS Spectrum: The Cr<sup>3+</sup> Aqueous Solution Case. *Phys. Rev. B: Condens. Matter Mater. Phys.* **2001**, *64*, 012201.
- (30) Ramírez-Solís, A.; Amaro-Estrada, J. I.; Hernández-Cobos, J.; Maron, L. Aqueous Solvation of SmI<sub>2</sub>: A Born-Oppenheimer Molecular Dynamics Density Functional Theory Cluster Approach. *Inorg. Chem.* **2018**, *57*, 2843–2850.
- (31) Rehr, J. J.; Kas, J. J.; Vila, F. D.; Prange, M. P.; Jorissen, K. Parameter-Free Calculations of X-Ray Spectra with FEFF9. *Phys. Chem. Chem. Phys.* **2010**, *12*, 5503–5513.
- (32) Zhao, G. J.; Liu, J. Y.; Zhou, L. C.; Han, K. L. Site-Selective Photoinduced Electron Transfer from Alcoholic Solvents to the Chromophore Facilitated by Hydrogen Bonding: A New Fluorescence Quenching Mechanism. *J. Phys. Chem. B* **2007**, *111*, 8940–8945.
- (33) Austin, A.; Petersson, G. A.; Frisch, M. J.; Dobek, F. J.; Scalmani, G.; Throssell, K. A Density Functional with Spherical Atom Dispersion Terms. *J. Chem. Theory Comput.* **2012**, *8*, 4989–5007.
- (34) Parr, R. G.; Yang, W. *Density-Functional Theory of Atoms and Molecules*; Oxford University Press: New York, 1989.
- (35) Paradas, M.; Campana, A. G.; Jimenez, T.; Robles, R.; Oltra, J. E.; Bunuel, E.; Justicia, J.; Cardenas, D. J.; Cuerva, J. M. Understanding the Exceptional Hydrogen-Atom Donor Characteristics of Water in Ti III -Mediated Free-Radical Chemistry. *J. Am. Chem. Soc.* **2010**, *132*, 12748–12756.
- (36) Pappas, I.; Chirik, P. J. Ammonia Synthesis by Hydrogenolysis of Titanium-Nitrogen Bonds Using Proton Coupled Electron Transfer. *J. Am. Chem. Soc.* **2015**, *137*, 3498–3501.
- (37) Tarantino, K. T.; Miller, D. C.; Callon, T. A.; Knowles, R. R. Bond-Weakening Catalysis: Conjugate Aminations Enabled by the Soft Homolysis of Strong N-H Bonds. *J. Am. Chem. Soc.* **2015**, *137*, 6440–6443.
- (38) Semproni, S. P.; Milsman, C.; Chirik, P. J. Four-Coordinate Cobalt Pincer Complexes: Electronic Structure Studies and Ligand Modification by Homolytic and Heterolytic Pathways. *J. Am. Chem. Soc.* **2014**, *136*, 9211–9224.
- (39) King, A. E.; Huffman, L. M.; Casitas, A.; Costas, M.; Ribas, X.; Stahl, S. S. Copper-Catalyzed Aerobic Oxidative Functionalization of an Arene C-H Bond: Evidence for an Aryl-Copper(III) Intermediate. *J. Am. Chem. Soc.* **2010**, *132*, 12068–12073.
- (40) Chalkley, M. J.; Oyala, P. H.; Peters, J. C. Cp\* Noninnocence Leads to a Remarkably Weak C-H Bond via Metallocene Protonation. *J. Am. Chem. Soc.* **2019**, *141*, 4721–4729.